Multiplexed stimulated emission depletion nanoscopy (mSTED) for 5-color live-cell long-term imaging of organelle interactome

Yuran Huang[1,†], Zhimin Zhang[1,2,†], Wenli Tao[1,†], Yunfei Wei[3], Liang Xu[1], Wenwen Gong[1], Jiaqiang Zhou[4], Liangcai Cao[5], Yong Liu[6], Yubing Han[1,3]*, Cuifang Kuang[1,2,7]* and Xu Liu[1,2]

[1]State Key Laboratory of Extreme Photonics and Instrumentation, College of Optical Science and Engineering, Zhejiang University, Hangzhou 310027, China; [2]Research Center for Intelligent Chips and Devices, Zhejiang Lab, Hangzhou 311121, China; [3]Wuhan National Laboratory for Optoelectronics, Huazhong University of Science and Technology, Wuhan 430074, China; [4]Department of Endocrinology and Metabolism, Sir Run Run Shaw Hospital, Zhejiang University School of Medicine, Hangzhou 310016, China; [5]Department of Precision Instruments, Tsinghua University, Beijing 100084, China; [6]College of electronics and information engineering, Shanghai University of Electrical Power, Shanghai 200090, China; [7]ZJU-Hangzhou Global Scientific and Technological Innovation Center, Hangzhou 311200, China.

[†]These authors contributed equally to this work.

*Correspondence: YB Han, E-mail: hanyubing@zju.edu.cn; CF Kuang, E-mail: cfkuang@zju.edu.cn

This file includes:

Supplementary information for this paper is available at https://doi.org/10.29026/oea.2024.240035
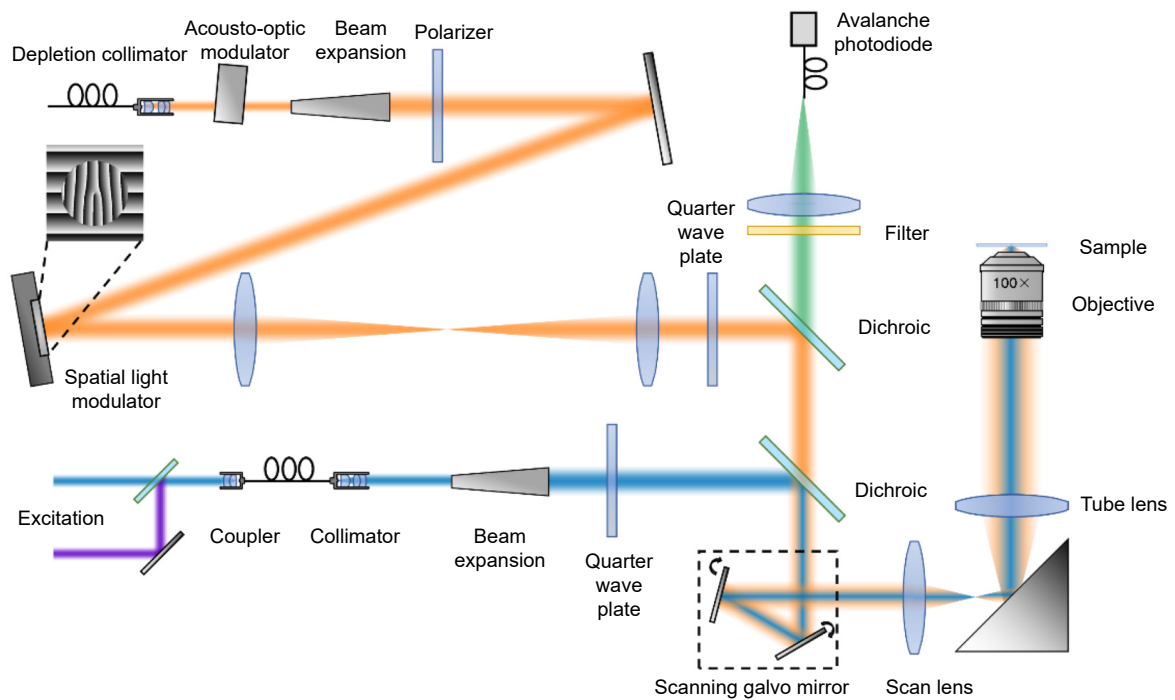
Fig. S1 | Stimulated emission depletion microscopy (STED) system setup strategy. Two pulsed excitation beams with wavelengths of 560 nm and 640 nm are coupled into a single-mode fiber, which is collimated and expanded at the other end of the fiber to reach a dichroic mirror; 775 nm depletion beam from a high-power pulsed laser is similarly expanded and collimated, and then modulated by a spatial light modulator. The spatial light modulator is loaded with a 0-2π vortex phase pattern superimposed on a sparkle grating pattern, thus separating the modulated depletion beam from the unmodulated portion. The modulated depletion beam is bundled with the excitation beam and passed through a galvanometer to scan the sample, while the fluorescence emitted from the sample is transmitted through the dichroic mirror and collected by a multi-mode fiber and an avalanche photodiode.
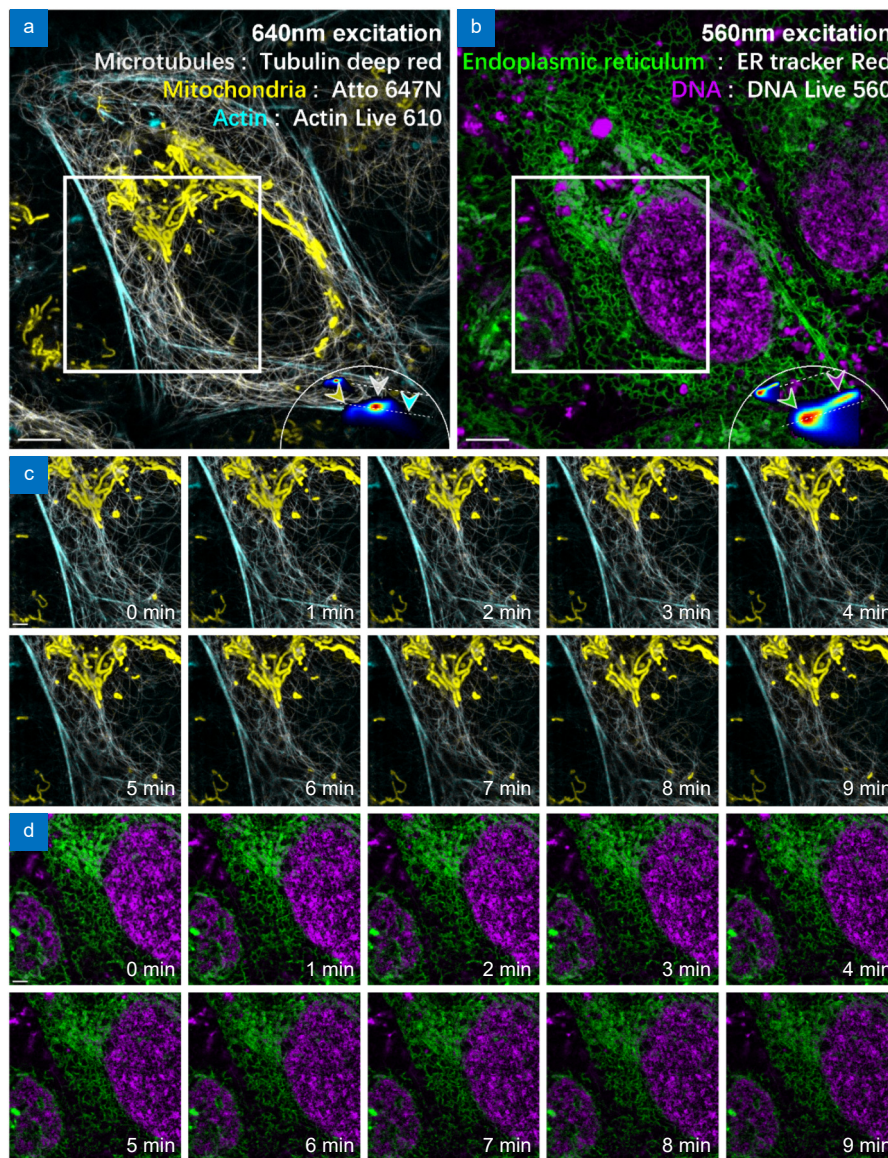
Fig. S2 | (**a**, **b**) Five-color imaging with dual excitation beams, multiplexing under 640 nm excitation and 560 nm excitation. (**c**, **d**) Cellular activity in the area within the white box in (a, b) during 9 min. Local residual crosstalk between microtubules and actin occurs due to insufficient lifetime differences, and we believe that enhanced labeling methods may help to address this issue. Scale bars: (a, b) 5 μm; (c, d) 2 μm
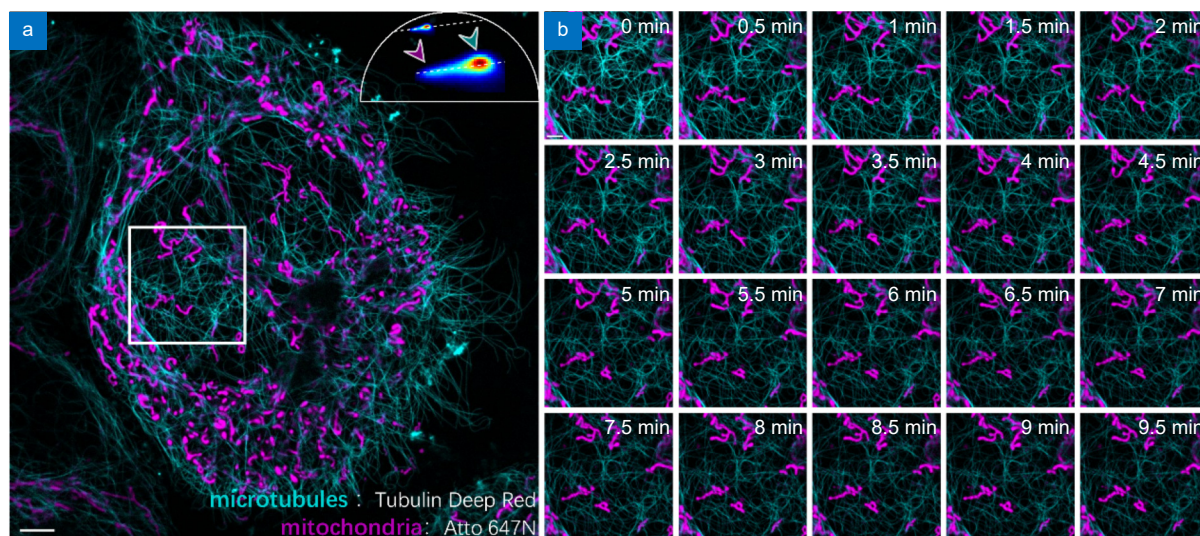
Fig. S3 | 2-color live cell imaging. (**a**) Lifetime multiplexed STED imaging results of microtubules (labeled withTubulin Deep Red) and mitochondria (labeled with Atto 647N). (**b**) Cellular activity in the area within the white box in (a) during 9.5 min. Mitochondrial movement, fusion and division along microtubules can be observed. Scale bars: (a) 5 μm; (b) 2 μm.

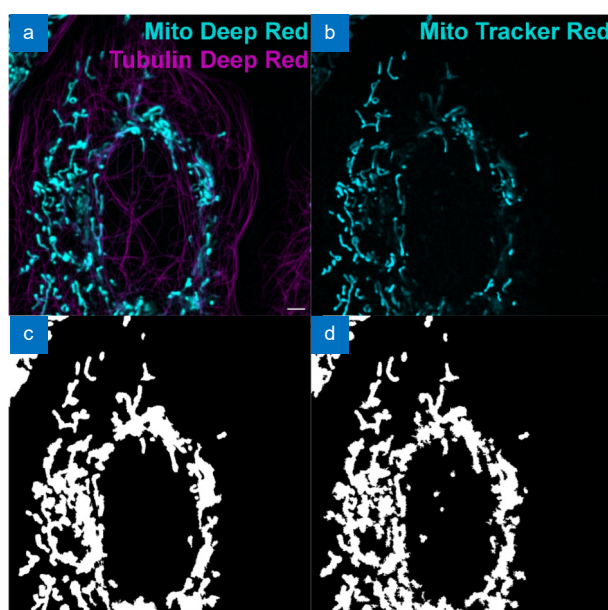

Fig. S4 | Verification of the accuracy of the segmentation results. (**a**) Mitochondria and microtubules were labeled withMito Deep Red and Tubulin Deep Red in the 640-nm excitation channel. (**b**) Mitochondria were labeled with Mito Tracker Red in the 560-nm excitation channel. (**c**, **d**) Dichotomization results for mitochondria in (a–b) with 4% difference in area. Scale bar: 5 μm.
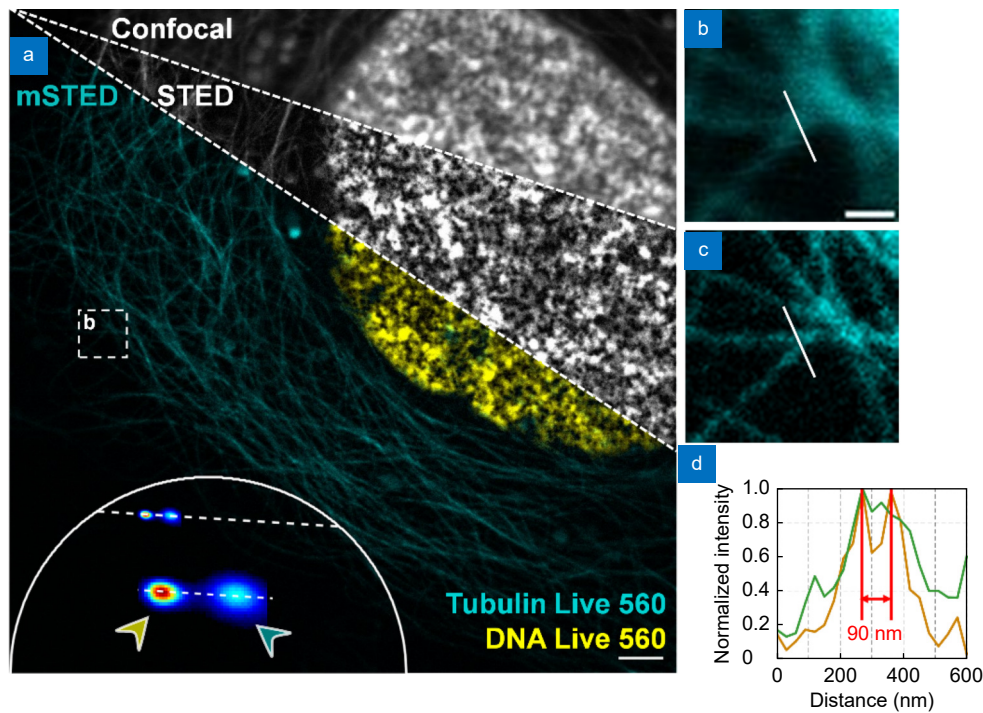
Fig. S5 | (**a**) mSTED of the 560-nm excitation channel, the grayscale image represents live cells imaged by Confcal and STED, whereas the color image is the mSTED result. The two structures were labeled withTubulin Live 560 and DNA Live 560, respectively. (**b**, **c**) Comparison of mSTED imaging with confocal imaging, corresponding to the regions marked by white boxes in (a). (**d**) Line profiles along the white line in (b, c), with the appearance of sharp peaks indicating a resolution of 90 nm for mSTED images of the 560-nm excitation channel. Scale bars: (a) 2 μm; (b, c) 500 nm.
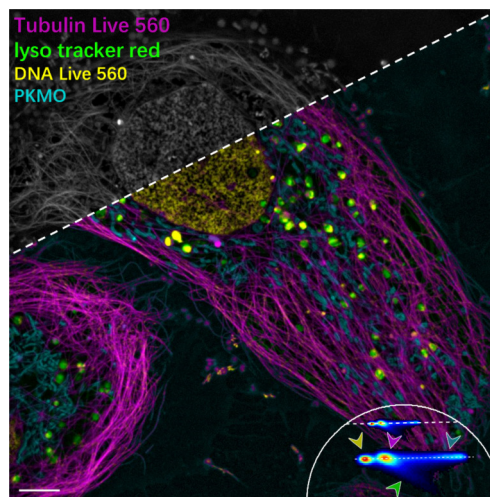

Fig. S6 | Four-color imaging with single excitation beam. Four structures were labeled simultaneously, with microtubules, mitochondria, and DNA labeled as in Fig. 3, and lysosomes labeled using lyso tracker red. The phasor clusters corresponding to lysosomes were extracted separately, and the remaining phasor points were later analyzed following the same method as in Fig. 3. Due to the unstable microenvironment inside the lysosome, some pixels belonging to the lysosome were incorrectly classified as DNA, but most of the area in the field of view maintained the correct separation. We believe that with more appropriate labeling methods, it is possible to achieve more discriminatory 4-color imaging in live cells using single excitation beam. Scale bar: 5 μm.
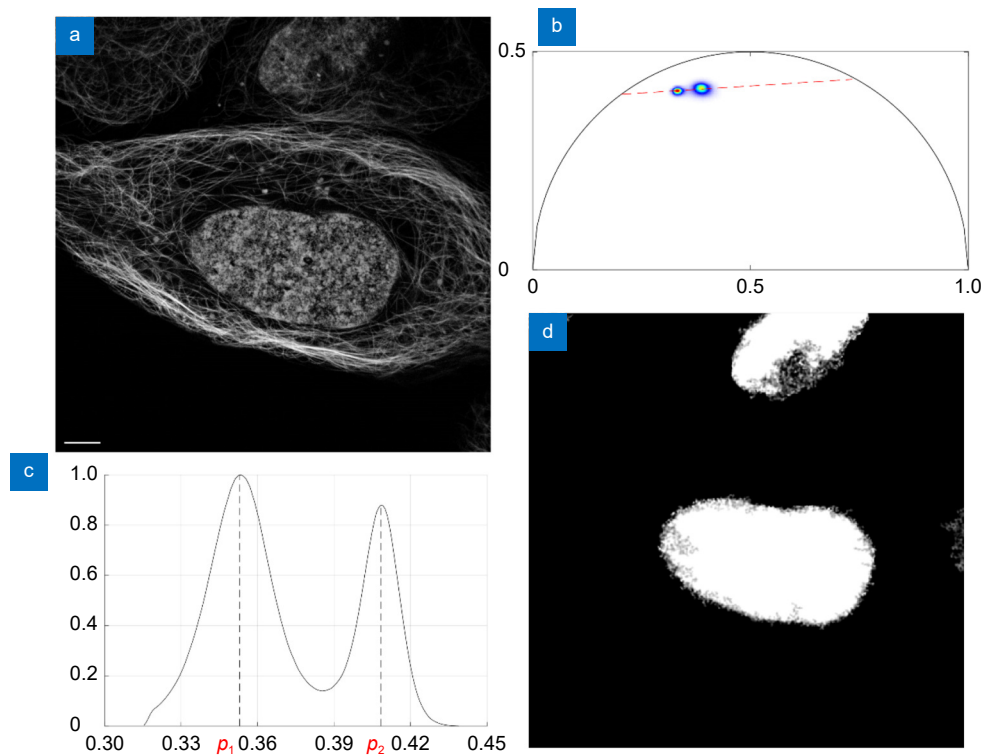
Fig. S7 | Separation of different structures by phasor plot. (**a**, **b**) Intensity imaging results and the corresponding phasor plots of TU Live 560-labeled microtubules and DNA Live 560-labeled DNA. (**c**) Curves obtained by projecting the phasor points in (b) onto the red fitting line. The *x*-axis represents the distance from the projection point to the intersection of the fitted line with the universal semicircle, the *y*-axis denotes the normalized number of pixels, and the peaks of the curves are labeled p_1 and p_2, corresponding to two distinct types of structures. (**d**) Mask calculated from (c) to multiply with the intensity image and obtain the DNA image and the microtubule image. Scale bar: 5um.

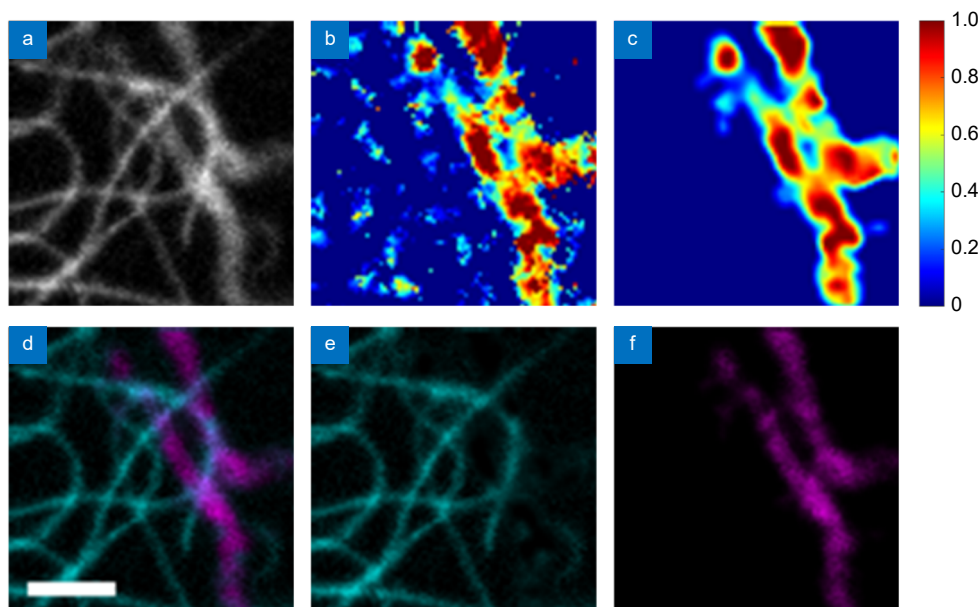**Fig. S8 | Separation of overlapping regions.** (**a**) Intensity map with mitochondria and microtubules overlapping each other. (**b**) Digital mask computed from the phasor points corresponding to each pixel. (**c**) Processed digital mask. (**d–f**) Overlay maps of mitochondria and microtubules and separate images. Microtubules and mitochondria are labeled with Docetaxel SiR and Atto 647N, respectively. scale bar: 1 μm.
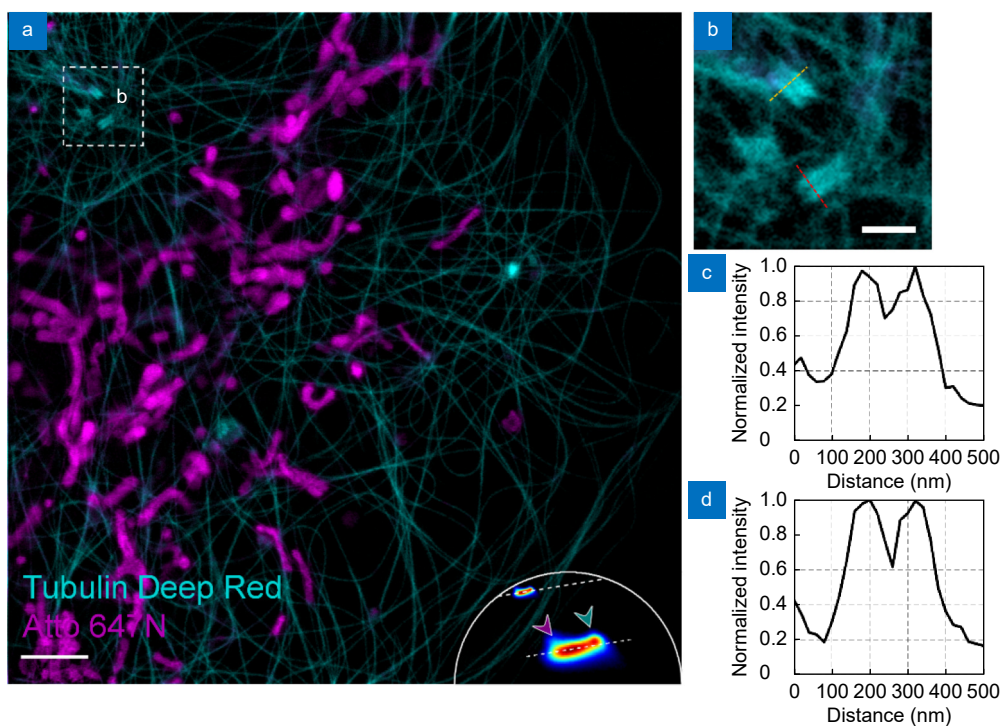
Fig. S9 | Centrosome imaging. (**a**) mSTED in the centrosome region. Live U2OS cells were labeled with Atto 647N (magenta; mitochondria) and Tubulin Deep Red (cyan; centrosomes and microtubules). The high-density Tubulin Deep Red probes in the centrosome region show similar lifetimes to those in the microtubule region, allowing them to be distinguished from Atto 647N. (**b**) Enlarged view of the regions marked by the white boxes in (a). The hollow structure of the centrosome could be resolved. (**c–d**) Normalized intensity distribution results along the orange end red dotted lines in (b), respectively. Both of them show two discrete peaks. Scale bars: (a) 2 μm; (b) 500 nm
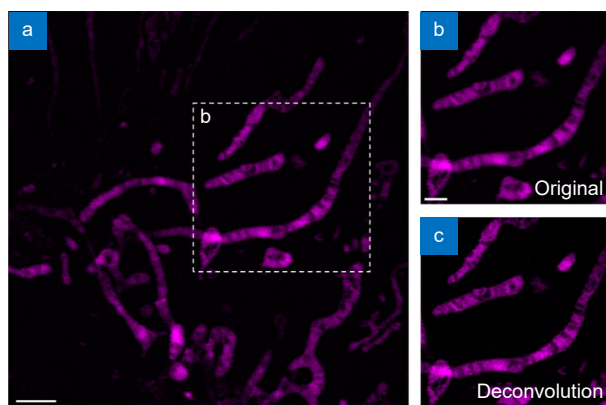

Fig. S10 | Mitochondrial cristae imaging. (**a**) Mitochondrial cristae in live COS-7 cells stained with PK Mito Orange. (**b**) Enlarged view of the regions marked by the white boxes in (a). (**c**) Richardson-Lucy deconvolution results for the same region in (b). Scale bars: (a) 2 μm; (b) 1 μm
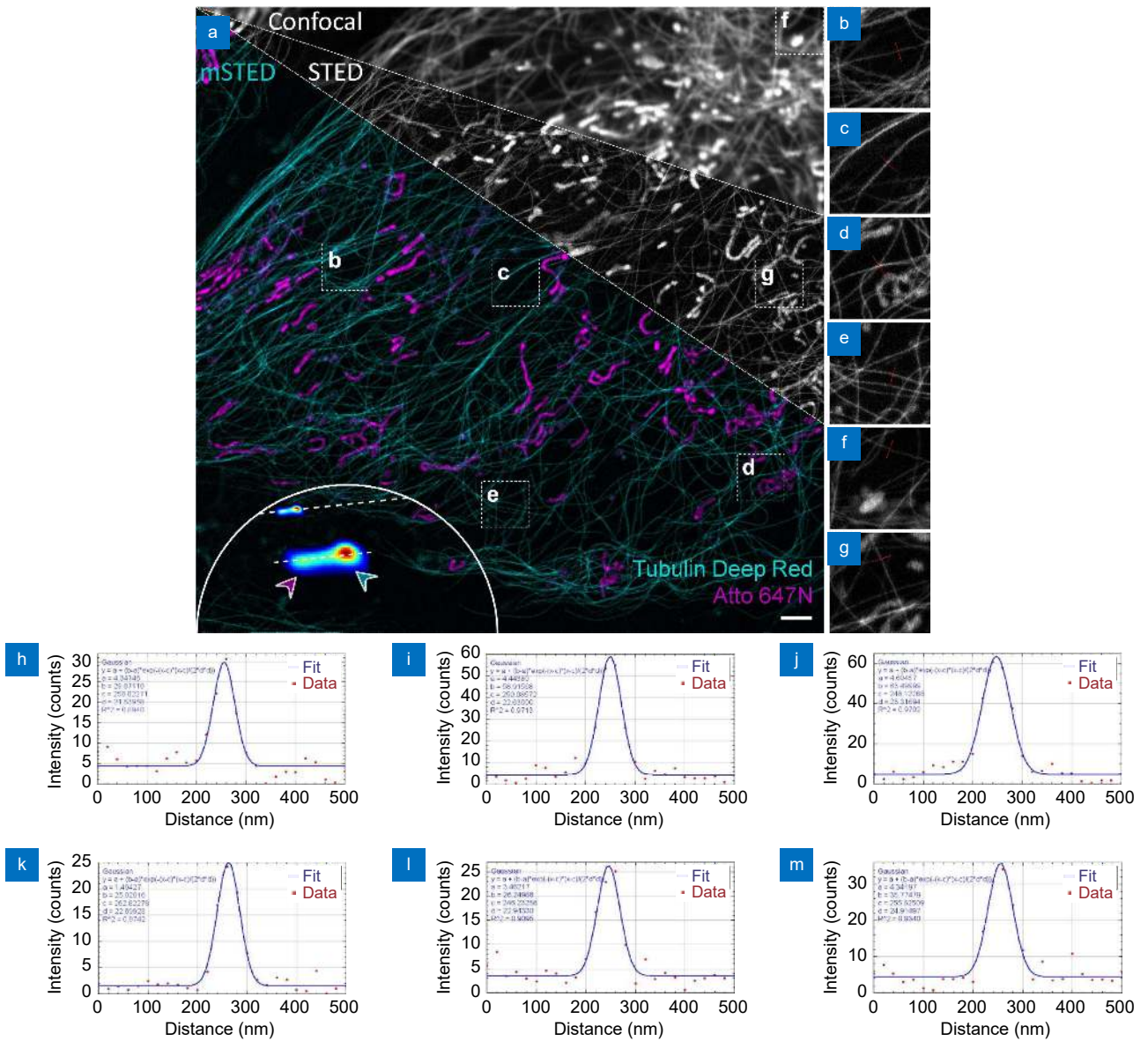
Fig. S11 | Microtubule diameter under mSTED. (**a**) mSTED image. Live U2OS cells were labeled with Atto 647N (magenta; mitochondria) and Tubulin Deep Red (cyan; microtubules). (**b–g**) Enlarged view of the regions marked by the white boxes in (a). (h–m) Intensity distribution and corresponding Gaussian fitting results along the dotted lines in (b–g). The diameter of the microtubules is 56 ± 5.8 nm, which matches the resolution of 60 nm. Scale bars: (a) 2 μm; (b) 500 nm

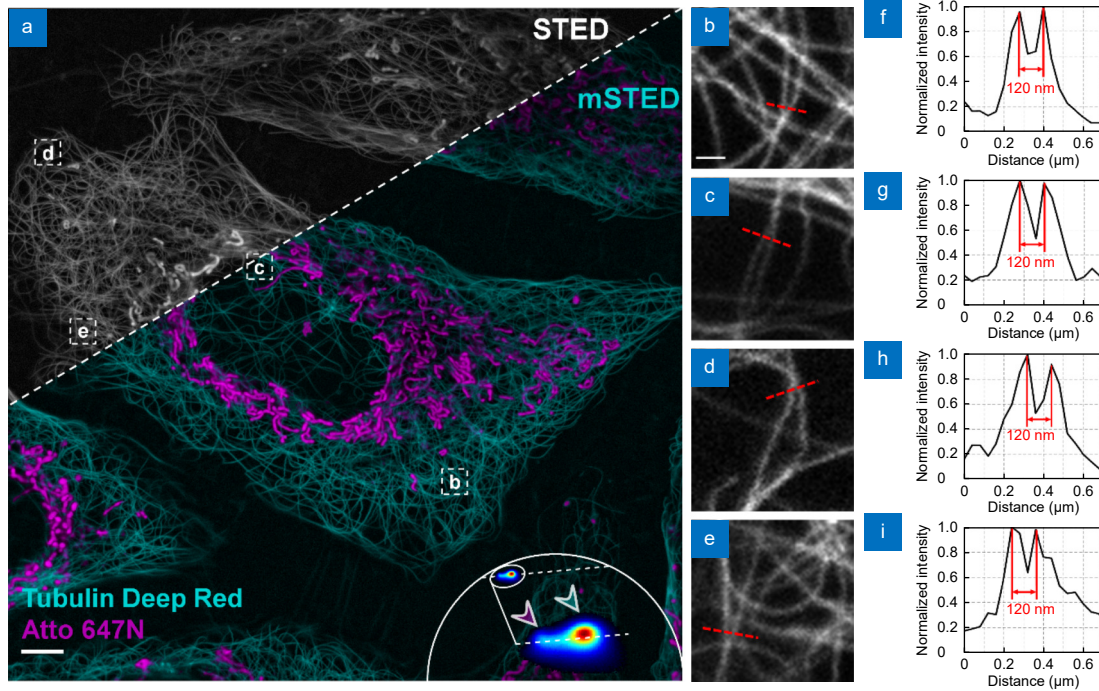**Fig. S12 | mSTED under low depletion intensity.** (**a**) mSTED image obtained at a depletion power density of 5.5 kW/cm². Live U2OS cells were labeled with Atto 647N (magenta; mitochondria) and Tubulin Deep Red (cyan; microtubules). (**b**–**e**) Enlarged view of the regions marked by the white boxes in (a). (**f**–**i**) Line profiles along the dotted lines in (b–e) which show a resolution of 120 nm for mSTED at this low depletion power density. Scale bars: (a) 5 μm; (b) 500 nm

Section 1: Measurement, transform and calibration method of fluorescence decay

In this section, we describe how to measure the fluorescence decay and remove the influence of Instrument Response Function (IRF) from it. The fluorescence decay consists of a histogram of photon arrival times, which can be obtained simply by adding time-correlated single photon counting (TCSPC) to a normal pulsed STED system. Generally, TCSPC requires three inputs: excitation beam pulse signal, fluorescence pulse signal, and pixel switching signal. In a pulsed STED system, all pulsed excitation beams and pulsed depletion beam are triggered by the same source, commonly comes from one of the lasers and is connected to the other lasers through a signal repeater and a signal delayer. A similar structure is also applied to the TCSPC. The fluorescence pulse signal comes from the APD, and in a normal point-scanning system the acquisition card is responsible for analyzing this signal, while in fluorescence lifetime imaging this signal is fed into the TCSPC, which obtains the relative arrival time of the photons by comparing the excitation light pulse signal with the fluorescence pulse signal. With the help of the pixel switching signal, the arrival time can be assigned to individual pixels.

The fluorescence decay is then transformed into the coordinates of the phase plot by the following equations[S1]:

$$g_{i,j} = \int_{t_0}^{T} D_{i,j}(t) \cdot \cos(\omega t) \mathrm{d}t \Big/ \int_{t_0}^{T} D_{i,j}(t) \mathrm{d}t \,, \tag{S1}$$

$$s_{i,j} = \int_{t_0}^{T} D_{i,j}(t) \cdot \sin(\omega t) \mathrm{d}t \Big/ \int_{t_0}^{T} D_{i,j}(t) \mathrm{d}t \,, \tag{S2}$$

where $D_{i,j}(t)$ is the fluorescence decay at pixel i, j, while $g_{i,j}$ and $s_{i,j}$ denote the horizontal and vertical coordinates of the corresponding phasor point. T and ω are the interval time and angular frequency of pulse excitation, respectively. t_0 is a time gate corresponding to the peak of fluorescence decay, which means that the rising edge is rejected.

If the fluorescence decay is mono-exponential, the transformed phase point will be located on the universal semicircle, while the phase point corresponding to multi-exponential attenuation will be located inside the universal semicircle. Ideally, the phasor points from the same fluorescent dye are all located at the same position in the phasor map, but actual imaging conditions are influenced by noise and microenvironment, and the phasor points will form a cluster. In mul-

ticolor imaging, the phasor map consists of multiple clusters.

If we measure a sample with a known mono-exponential fluorescence decay, we find that the phasor point does not lie directly on the universal semicircle because the actual measured fluorescence decay is related to the IRF, which is mainly determined by the pulse width of the laser and is influenced by the detector and TCSPC. In time-domain lifetime imaging, the correction for IRF is done by deconvolution or discarding the leading segment of the fluorescence decay, while in the phasor plot method, the correction for IRF can be obtained by a simple mathematical transformation:

$$G_{i,j} = (g_{\mathrm{IRF}} \cdot g_{i,j} + s_{\mathrm{IRF}} \cdot s_{i,j})/(g_{\mathrm{IRF}}^2 + s_{\mathrm{IRF}}^2) \ , \tag{S3}$$

$$S_{i,j} = (- s_{\mathrm{IRF}} \cdot g_{i,j} + g_{\mathrm{IRF}} \cdot s_{i,j})/(g_{\mathrm{IRF}}^2 + s_{\mathrm{IRF}}^2) \ , \tag{S4}$$

in which $G_{i,j}$ and $S_{i,j}$ are the coordinate of the phasor point corrected for IRF; $g_{i,j}$ and $s_{i,j}$ denote the uncorrected coordinates, determined by fluorescence decay and excitation; g_{IRF} and s_{IRF} are calculated by

$$g_{IRF} = \int_{t_0}^{T} IRF(t) \cdot \cos(\omega t) \mathrm{d}t \Big/ \int_{t_0}^{T} D_{i,j}(t) \mathrm{d}t \ , \tag{S5}$$

$$s_{IRF} = \int_{t_0}^{T} IRF(t) \cdot \sin(\omega t) \mathrm{d}t \Big/ \int_{t_0}^{T} D_{i,j}(t) \mathrm{d}t \ . \tag{S6}$$

Section 2: Processing method for phasor plot

The objective of phasor plot processing is to generate a set of masks that assign fluorescent signals to multiple images representing different structures. This process is exemplified in Fig. S7, which illustrates the separation of fluorescent probes. In Fig. S7(a, b), the obtained intensity map is depicted by directly counting fluorescent photons, while the Phasor plot is obtained by measuring fluorescence decay. The two clusters observed in the Phasor plot correspond to DNA and microtubules. To simplify the illustration of the segmentation problem, we project the phasor plot onto a one-dimensional representation. The direction of the projection is determined through a linear fit. Figure S7(c) presents a histogram of the projected results, where the *x*-axis represents the distance from the projection point to the intersection of the fitted line with the universal semicircle. The *y*-axis denotes the normalized number of pixels, and the peaks of the curves are labeled as p_1 and p_2, corresponding to two distinct types of structures. It is important to note that if a certain structure occupies a small number of pixels, its peak may not be clearly visible. In such cases, the peak position associated with that structure can be pre-labeled through monochromatic imaging. Subsequently, the digital mask is computed using the following equation:

$$m_{i,j} = \begin{cases} 0 & p_{i,j} \leqslant p_1 \\ \dfrac{p_{i,j} - p_1}{p_2 - p_1} & p_1 < p_{i,j} < p_2 \\ 1 & p_{i,j} \geqslant p_2 \end{cases} \ . \tag{S7}$$

The mask may be locally biased due to noise or microenvironment variations, thus introducing crosstalk between structures. To alleviate this issue, binarized image processing is introduced to eliminate isolated points in the mask. The final result is presented in Fig. S7(d). By multiplying the intensity map with the mask, the DNA image (Fig. 1(k)) and microtubule image (Fig. 1(l)) are obtained.

Figure S8 serves as an additional example to visually demonstrate the process of separating different structures. Specifically, we selected a region where mitochondria and microtubules overlap locally, making it difficult to distinguish between these two structures based purely on the intensity map shown in Fig. S6(a). To address this challenge, we employed a series of steps. Firstly, we processed the phasor plot to generate a digital mask, depicted in Fig. S8(b). Subsequently, we eliminated isolated points and applied low-pass filtering, resulting in Fig. S8(c). By multiplying the digital mask with the intensity map, we successfully obtained separate images of microtubules and mitochondria, as displayed in Fig. S8(d–f). This procedure effectively highlights the distinct features of each structure and enables their accurate separation.

It is worth noting that the low-pass filtering processing of phasor points and digital masks includes a priori knowledge of continuity. This is based on the premise that in order to satisfy the Nyquist sampling criterion, the PSF of a fluo-

rescence image must occupy a certain number of pixels. Additionally, some of the structures themselves are of large size. In this case, a discontinuous variation of the pixel values is caused by noise. To ensure optimal results, it is recommended to adjust the diameter of the low-pass filter window to match the imaging PSF. The minimum diameter should be 3 pixels, which corresponds to the minimum size of the PSF in the image.
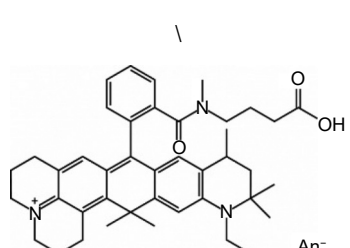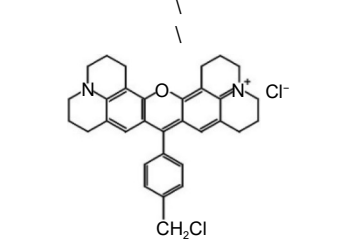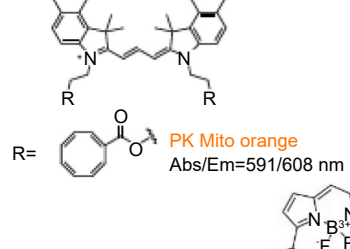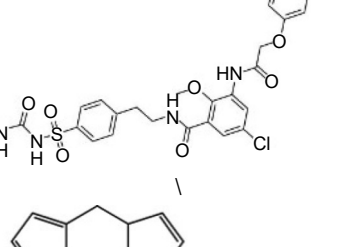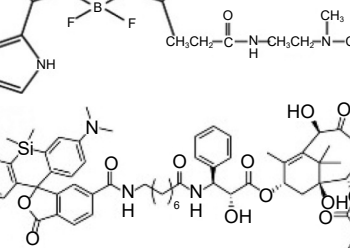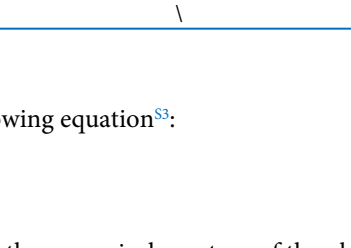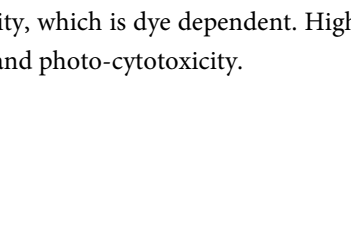
Section 3: Live-cell labeling

U2OS (human osteosarcoma cell line) cells were purchased from the American Type Culture Collection and cultured in McCoy's 5A medium (Cat.No:16600-082; Thermo Fisher Scientific, Inc.) supplemented with 10% (v/v) fetal bovine serum (FBS; Cat.No:10091-148; Thermo Fisher Scientific, Inc.). The cultures were maintained at 37°C in a humidified 5% CO2 environment and seeded into glass bottom dishes (Cat.No:81158; ibidi, GmbH.) at a density of $1.5\sim2.0 \times 10^4$ per well before labeling. After an overnight incubation, the cells were washed three times with PBS.

The work solutions of the live-cell probes were diluted with phenol red-free DMEM (Cat.No:31053-028; Thermo Fisher Scientific, Inc.). For commercially available probes, the cells were incubated with Tubulin Deep Red (dilution ratio 1:1000; Cat.No:C2215S; Beyotime Biotechnology), Tubulin Live 560 (1 μM; Cat.No:LV560-0141; Abbeiror), DNA Live 560 (1 μM; Cat.No:LV560-0143; Abbeiror), Mito Tracker Red (1 μM; Cat.No:C1035; Beyotime Biotechnology), PK Mito Orange (PKMO; 0.2 μM; Cat.No:PKMO-1; Genvivo), ER Tracker Red (1 μM; Cat.No:E34250; Invitrogen), Actin Live 610 (100nM; Cat.No:lv610-0140; Abbeiror), Docetaxel SiR (1 μM; Cat.No:CY-SC002; Cytoskeleton), Lyso Tracker Red (200 nM; Cat.No:C1046; Beyotime Biotechnology) in a 5% CO2 atmosphere at 37 °C for 30 min. For Atto 647N NHS ester (5 μM; Cat.No:18373; Sigma-Aldrich Co., LLC) labeling, an aliquot of the probe was dissolved in 10 μL of DMSO and was diluted with PBS to a total volume of 100 μL (3–6 μM), and the cells were then incubated with the probe solution in a 5% CO_2 atmosphere at 37 °C for 30 min. Nocodazole (5 μM; Cat.No:N129755; Aladdin) was added into the work solution of the probes to promote the depolymerization of microtubules in Fig. 3. The above probes and drug information can be accessed in Table S1.

Afterwards, the supernatant was discarded, and a solution of Trypan blue (100 μL, 1 mg·mL^{-1}; Cat.No:40724ES10; Sigma-Aldrich Co., LLC) in PBS was added to exclude the dead cells and quench the extracellular fluorescence from the probes[S2]. After incubation for 1 min, Trypan blue was removed, and the cells were washed twice gently with PBS and immersed in phenol red-free DMEM prior to optical imaging.

Table S1 | Probes and drug for mSTED.

Probe	Producers	Catalog number	Dosage	Structure
Tubulin Deep Red	Beyotime biotechnology	C2215S	Dilution ratio 1：1000	
Atto 647N	Sigma-Aldrich	18373	5 μM	
Tubulin Live 560	Abberior	LV560-0141	1 μM	
DNA Live 560	Abberior	LV560-0143	1 μM	
Mito tracker Red	Beyotime Biotechnology	C1035	1 μM	
PK Mito Orange	Genvivo	PKMO-1	0.2 μM	
ER tracker Red	Invitrogen	E34250	1 μM	
Actin Live 610	Abberior	LV610-0140	100 nM	
Lyso tracker Red	Beyotime Biotechnology	C1046	200 nM	
Tubulin SiR	Cytoskeleton	CY-SC002	1 μM	
Nocodazole	Aladdin	N129755	5 μM	

Section 4: Relationship between resolution and depletion intensity

In general, the resolution and depletion power density of mSTED satisfy the following equation[S3]:

$$d = \frac{\lambda}{2NA\sqrt{1 + I_{max}/I_s}} \, ,$$

where *d* is the resolution, *λ* denotes the wavelength of the excitation beam, *NA* is the numerical aperture of the objective lens, I_{max} denotes the depletion intensity, and I_s represents the saturation intensity, which is dye dependent. Higher depletion intensity results in higher resolution, but also increases photo-bleaching and photo-cytotoxicity.

References

S1. Ranjit S, Malacrida L, Jameson DM et al. Fit-free analysis of fluorescence lifetime imaging data using the phasor approach. *Nat Protoc* **13**, 1979–2004 (2018).

S2. Manceur A, Wu A, Audet J. Flow cytometric screening of cell-penetrating peptides for their uptake into embryonic and adult stem cells. *Anal Biochem* **364**, 51–59 (2007).

S3. Hell SW. Far-field optical nanoscopy. *Science* **316**, 1153–1158 (2007).